Structural Roles for Human Translation Factor eIF3 in Initiation of Protein Synthesis

Bunpote Siridechadilok,[1] Christopher S. Fraser,[1,3]* Richard J. Hall,[4]* Jennifer A. Doudna,[1,2,3,4]† Eva Nogales[1,3,4]†

Protein synthesis in mammalian cells requires initiation factor eIF3, a ~750-kilodalton complex that controls assembly of 40*S* ribosomal subunits on messenger RNAs (mRNAs) bearing either a 5′-cap or an internal ribosome entry site (IRES). Cryo–electron microscopy reconstructions show that eIF3, a five-lobed particle, interacts with the hepatitis C virus (HCV) IRES RNA and the 5′-cap binding complex eIF4F via the same domain. Detailed modeling of eIF3 and eIF4F onto the 40*S* ribosomal subunit reveals that eIF3 uses eIF4F or the HCV IRES in structurally similar ways to position the mRNA strand near the exit site of 40*S*, promoting initiation complex assembly.

Protein synthesis begins with recruitment of an mRNA to the small ribosomal subunit before the formation of active ribosomes (*1*). In mammalian cells, translation initiation factor eIF3 binds 40*S* subunits and recruits mRNAs bearing a methylated guanosine cap at the 5′-end (5′-m7G cap) via direct interaction with the 5′-cap binding complex eIF4F (*1*, *2*). Many viral mRNAs, however, use a structured RNA element, or IRES, that interacts with eIF3 and functionally replaces the mRNA 5′-cap and all or part of the cap binding complex (*3*). Comprising at least 12 proteins in humans, eIF3 also prevents premature association of the 40*S* and 60*S* ribosomal subunits, interacts with other initiation factors that detect the start codon, and helps assemble active ribosomes (*1*, *2*). Despite its importance in both cellular and viral protein synthesis initiation, the structural bases for eIF3 activities and interactions with the translational machinery are unknown.

To obtain a structure of eIF3, we produced an initial electron microscopy (EM) reconstruction using the random-conical tilt method on negatively stained human eIF3 samples (*4*, *5*). This reconstruction was then used as a reference for projection matching of cryo-EM data to produce an improved reconstruction at ~30 Å resolution (Fig. 1A) (*5*, *6*). The largest dimension of eIF3 is ~175 Å, with individual domains ranging between 60 and 100 Å in length. eIF3 shows anthropomorphic features that have been used to name the five domains according to body parts, including a head, arms, and legs (Fig. 1A). The front surface of the complex is rather flat, whereas the back contains a cleft separating the domains into two slabs of density.

This structure must interact with RNA and protein factors to organize the assembly of the translation initiation complex. In the hepatitis C virus, the uncapped mRNA contains an IRES in its 5′-untranslated region that binds directly to eIF3 to form part of the ternary complex necessary for viral protein synthesis (*7*–*9*). The IRES circumvents the need for eIF3 binding to initiation factor eIF4G, a component of eIF4F, which is essential to position the 5′-end of the transcript on the ribosome during translation initiation on most cellular mRNAs (*10*).

We used cryo-EM and difference mapping to locate the HCV IRES binding site on eIF3. Initial two-dimensional (2D) analysis of eIF3-IRES showed extra density extending from the left arm of eIF3 (Fig. 1B, left panel) (*5*). We used projection-matching to the unliganded eIF3 structure, together with common-line cross-correlation between class averages corresponding to different views, to assign the particles to one of three IRES conformational groups (*5*, *11*). From this analysis, three reconstructions were produced representing the full range of observed IRES conformations (Fig. 1B). One of these reconstructions, corresponding to the most abundant IRES conformer (Fig. 1B, conformer-1), shows a hook-like density for the IRES protruding from the left arm of eIF3. The difference map between refined conformer-1 and unliganded eIF3 corresponds well to the HCV IRES density observed in a previous reconstruction of the HCV IRES-40*S* complex (Fig. 2A) (*5*, *12*). This analysis reveals that the IRES extends across eIF3, from the left arm to the right leg (Fig. 2A). On the basis of previous mapping of RNA helices onto the IRES density, domain IIId/e/f of the IRES appears to be located near the central region of eIF3, domain IIIa/b/c is near the right leg, and domain II corresponds to the flexible region emanating from the left arm of eIF3 (*12*). The extended interaction surface between the

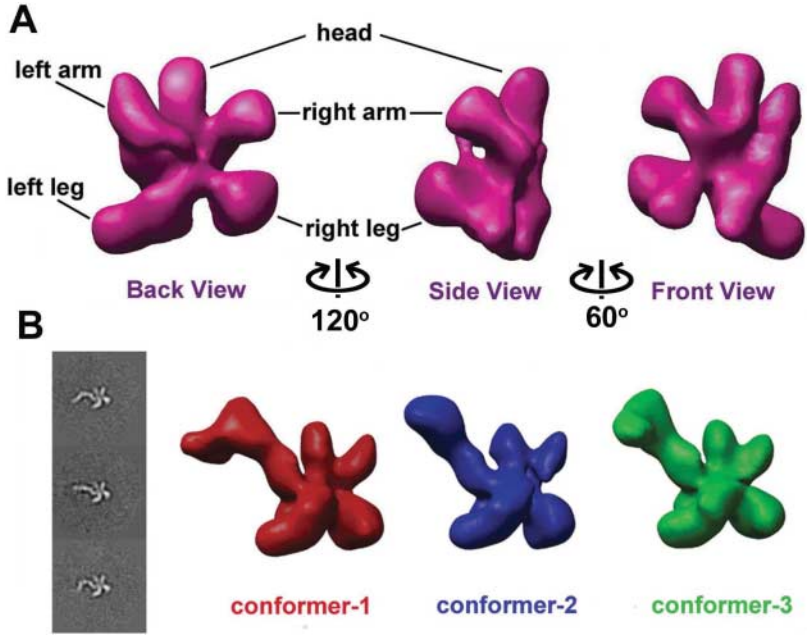

Fig. 1. Cryo-EM reconstructions of eIF3 and eIF3-IRES. (**A**) eIF3 at ~30 Å resolution [by 0.5 Fourier shell correlation function (FSC) cutoff]. (**B**) eIF3-IRES class averages showing flexible HCV-IRES (left) and corresponding 3D models (back view of eIF3 toward the viewer). The refined conformer-1 was used for difference mapping and modeling.

[1]Department of Molecular and Cell Biology, [2]Department of Chemistry, [3]Howard Hughes Medical Institute, University of California, Berkeley, CA 94720, USA. [4]Lawrence Berkeley National Laboratory, Berkeley, CA 94720, USA.

*These authors contributed equally to this work.
†To whom correspondence should be addressed. E-mail: enogales@lbl.gov (E.N.); doudna@berkeley.edu (J.A.D.)

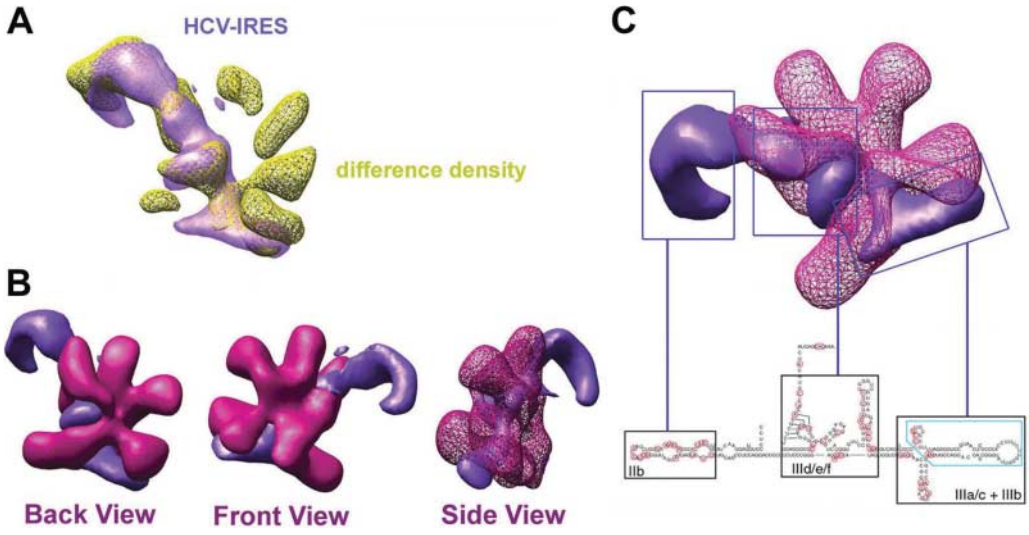

Fig. 2. Mapping of IRES domain interactions with eIF3. (**A**) Difference map between eIF3-IRES conformer-1 (Fig. 1B) and eIF3 (yellow mesh) and its superposition with the HCV-IRES density from the 40*S*-IRES study (transparent blue surface) (*12*). (**B**) Composite of eIF3 density and HCV-IRES density. (**C**) Predicted position of IRES domains in relation to eIF3 structure, based on previous mapping (*12*).

IRES and eIF3 agrees with biochemical studies in which at least four subunits of eIF3 (eIF3a, -b/c, -d, and -f) could be cross-linked to the IRES (*7*). Modification interference and footprinting assays that identified the IRES domain IIIa/b/c (Fig. 2C) as the primary binding site for eIF3 may have underrepresented weaker or more dynamic interaction sites (*7*, *13*). Notably, the difference map also includes extra densities (Fig. 2A) that suggest conformational changes in the right arm and right leg domains of eIF3 upon IRES binding.

By superimposing the structure of eIF3-IRES (Fig. 2B) onto a previous cryo-EM reconstruction of 40*S*-IRES using the IRES density, we produced a model of the 40*S*-eIF3-IRES complex that illustrates the interaction of eIF3 with 40*S* (Fig. 3, A and B) (*12*). This ternary model lacks any physical overlap of the components, showing excellent surface complementarity between eIF3 and the functionally critical 40*S* platform. The location and orientation of eIF3 on 40*S* is further supported by 2D difference mapping of negatively stained 40*S*-eIF3 complex and 40*S* alone (Fig. 3C) and by a previous low-resolution reconstruction of rabbit 40*S*-eIF3 (*5*, *14*). The eIF3 mass in the ternary complex localizes to the solvent-exposed side of 40*S*, where the front surface of eIF3 contacts 40*S*. The front of the eIF3 left leg sits below the platform near the 60*S* subunit interface, whereas the left arm points toward the tRNA exit (E) site (Fig. 3, A and B). The relative positions of 40*S*, eIF3, and IRES in our model (Fig. 2B, side view; Fig. 3, A and B) make it unlikely that IRES binding to 40*S* or eIF3 takes place after 40*S*-eIF3 binding.

The position of eIF3 in the 40*S*-eIF3-IRES model provides a plausible explanation for its role in preventing premature joining of 40*S* and 60*S* subunits. Structural and biochemical studies of the bacterial and eukaryotic ribosomes revealed two critical intersubunit contacts (B4 and B2a) involving binding of the small subunit protein S15/rpS13 to helix 34 of the large subunit (B4) and interaction between the small subunit helix 44 and helix 69 of the large subunit (B2a) (*15*–*17*). Our model suggests that the left toe of eIF3 covers the small subunit protein S15/rpS13, likely preventing the helix 34 contact (Fig. 3B). Fur-

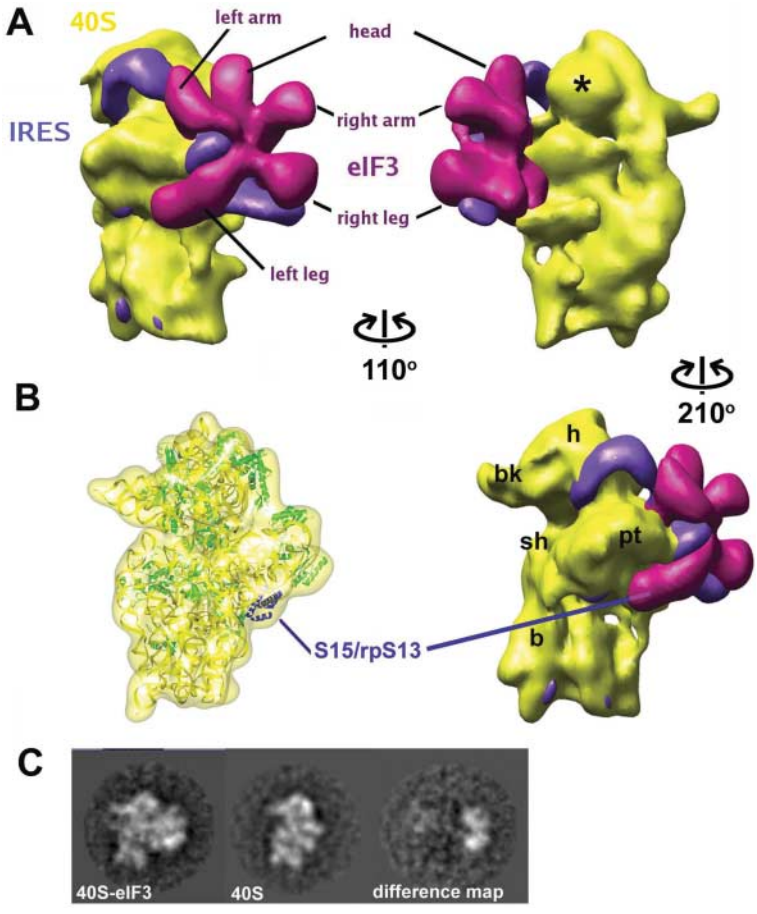

Fig. 3. 40*S*-eIF3-IRES model. (**A**) Views of the 40*S*-eIF3-IRES model; location of RACK1 is indicated by an asterisk. (**B**) 30*S* crystal structure from *T. thermophilus* (*31*) (left, hybrid model) and equivalent view of 40*S*-eIF3-IRES model (right) (b, body; bk, beak; h, head; pt, platform; sh, shoulder). (**C**) EM analysis of 40*S* binding to eIF3, showing class averages in the same orientation from particles with and without bound eIF3.

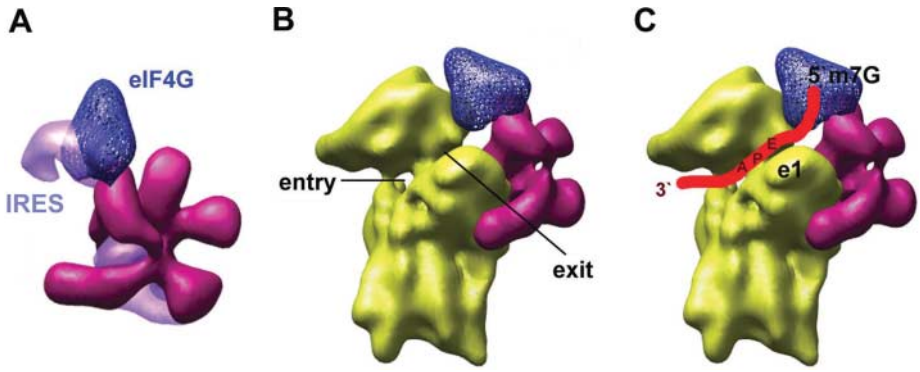

Fig. 4. Mapping of the eIF4G binding site on eIF3 and model of 40*S* complex with eIF3, eIF1, mRNA, and eIF4G. (**A**) Superposition of eIF4G density from difference mapping on the eIF3-IRES. (**B**) Model based on Fig. 4A and Fig. 3. The mRNA entry and exit sites are indicated. (**C**) Model of mRNA loading; e1 indicates eIF1 position (*21*). The A, P, and E sites are indicated. mRNA is depicted as a red line.

thermore, eIF3 may stabilize the binding of other conserved initiation factors that occlude the B2a interface contact, as suggested by a recent cryo-EM reconstruction of a prokaryotic initiation complex (*18*) and biochemical analysis of eukaryotic initiation complex assembly (*19*).

To determine how the HCV IRES might functionally replace eIF4G during translation initiation, we used EM and difference mapping to locate the eIF4G binding site on eIF3. Two-dimensional difference maps generated by comparing class-averages of eIF3-eIF4G and eIF3 alone showed an extra mass located near the eIF3 left arm (fig. S5). The class averages were used for back-projection to reconstruct a low-resolution structure of the complex (*5*). The difference density between the eIF3-eIF4G complex and eIF3 shows extra density located at the tip of the left arm with a mass consistent with the size of eIF4G. Therefore, eIF4G binds to the same arm as that occupied by part of the HCV IRES in the eIF3-IRES complex (Fig. 4A).

The 40*S*-eIF3-IRES model allows us to infer the placement of eIF4G relative to 40*S* and other initiation factors, locating eIF4G very close to the E site (Fig. 4B) (movie S1). This analysis predicts the position of eIF4F and the approximate location of the 5′-m7G cap of an mRNA (Fig. 4C). The placement of the 5′-end of the mRNA near the E site agrees well with the polarity of the mRNA during decoding by the ribosome, in which the 5′-end protrudes from the E site while the 3′-end is pulled into the ribosome toward the decoding site (*20*). Furthermore, in this model, eIF1 (and its bacterial ortholog IF3), the C-terminal domain of which has been mapped to the platform area by chemical probing and cryo-EM, would be located within a reasonable distance to interact with both eIF4G and the left arm of eIF3 (*18*, *21*, *22*). The interaction between *Saccharomyces cerevisiae* eIF4G and eIF1, as well as the interactions between *S. cerevisiae* and mammalian eIF3 and eIF1, have been detected both in vitro and in vivo (*23*, *24*).

The position of eIF4F on eIF3 near the ribosomal E site has implications for both translation regulation and ribosome scanning of the 5′-untranslated region of a nascently bound mRNA during translation initiation (*25*). First, the location of the receptor for activated C-kinase (RACK1) on the head of 40*S* is close to the bound factors (Fig. 3A) (*26*). Because several subunits of eIF3 are phosphorylated in vivo (*27*), our model suggests that RACK1-associated kinases could regulate the function of eIF3 and eIF4F on the ribosome. Phosphorylation of eIF3 by these kinases could be a mode of regulation used during the initiation process. Second, the location of eIF4G near the E site implies that eIF4A, a subunit of eIF4F, binds near the lagging rather than the leading side of the bound mRNA. To initiate protein synthesis, 40*S* "scans" from the 5′-cap structure toward the start codon, requiring energy (in the form of adenosine triphosphate) which is most likely used by eIF4A, a canonical DEX/H-D helicase (*28*). Translation initiation is enhanced by eIF4A even in the absence of secondary structure in the 5′-untranslated region of the mRNA (*29*), and the ribosome itself has RNA unwinding activity (*30*). Therefore, placement of eIF4A near the E site suggests the interesting possibility that eIF4A may establish directionality by preventing the backward movement of the 40*S* ribosomal subunit as it moves toward the start codon.

Comparison of the 40*S*-eIF3-IRES and 40*S*-eIF3-eIF4G models suggests an intriguing similarity in the function of the HCV IRES and eIF4F to anchor the attached mRNA strand, in either case, near the exit site on the head of 40*S*. Such structurally analogous positioning implies mechanistic overlap of HCV IRES and eIF4F activities, possibly explaining why HCV does not need eIF4F for viral protein synthesis (*8*). Ribosome recruitment to an mRNA, a necessary first step in the protein biosynthetic process, thus appears to involve conserved interactions coordinated by eIF3 that correctly load the mRNA into the ribosomal decoding center and prepare 40*S* for assembly into active ribosomes.

References and Notes

1. J. W. B. Hershey, W. C. Merrick, in *Translational Control of Gene Expression*, N. Sonenberg, J. W. B. Hershey, M. B. Mathews, Eds. (Cold Spring Harbor Laboratory Press, New York, 2000), pp. 31–69.
2. L. D. Kapp, J. R. Lorsch, *Annu. Rev. Biochem.* **73**, 657 (2004).
3. C. U. Hellen, P. Sarnow, *Genes Dev.* **15**, 1593 (2001).
4. M. Radermacher, T. Wagenknecht, A. Verschoor, J. Frank, *J. Microsc.* **146**, 113 (1987).
5. See supporting data on *Science* Online.
6. P. A. Penczek, R. A. Grassucci, J. Frank, *Ultramicroscopy* **53**, 251 (1994).
7. D. V. Sizova, V. G. Kolupaeva, T. V. Pestova, I. N. Shatsky, C. U. Hellen, *J. Virol.* **72**, 4775 (1998).
8. T. V. Pestova, I. N. Shatsky, S. P. Fletcher, R. J. Jackson, C. U. Hellen, *Genes Dev.* **12**, 67 (1998).
9. J. S. Kieft, K. Zhou, R. Jubin, J. A. Doudna, *RNA* **7**, 194 (2001).
10. A. C. Gingras, B. Raught, N. Sonenberg, *Annu. Rev. Biochem.* **68**, 913 (1999).
11. R. J. Hall, B. Siridechadilok, E. Nogales, in preparation.
12. C. M. Spahn *et al.*, *Science* **291**, 1959 (2001).
13. J. S. Kieft *et al.*, *J. Mol. Biol.* **292**, 513 (1999).
14. S. Srivastava, A. Verschoor, J. Frank, *J. Mol. Biol.* **226**, 301 (1992).
15. G. M. Culver, J. H. Cate, G. Z. Yusupova, M. M. Yusupov, H. F. Noller, *Science* **285**, 2133 (1999).
16. U. Maivali, J. Remme, *RNA* **10**, 600 (2004).
17. C. M. Spahn *et al.*, *Cell* **107**, 373 (2001).
18. G. S. Allen, A. Zavialov, R. Gursky, M. Ehrenberg, J. Frank, *Cell* **121**, 703 (2005).
19. V. G. Kolupaeva, A. Unbehaun, I. B. Lomakin, C. U. Hellen, T. V. Pestova, *RNA* **11**, 470 (2005).
20. G. Z. Yusupova, M. M. Yusupov, J. H. Cate, H. F. Noller, *Cell* **106**, 233 (2001).
21. I. B. Lomakin, V. G. Kolupaeva, A. Marintchev, G. Wagner, T. V. Pestova, *Genes Dev.* **17**, 2786 (2003).
22. A. Dallas, H. F. Noller, *Mol. Cell* **8**, 855 (2001).
23. C. M. Fletcher, T. V. Pestova, C. U. Hellen, G. Wagner, *EMBO J.* **18**, 2631 (1999).
24. H. He *et al.*, *Mol. Cell. Biol.* **23**, 5431 (2003).
25. M. Kozak, *J. Cell Biol.* **108**, 229 (1989).
26. J. Sengupta *et al.*, *Nat. Struct. Mol. Biol.* **11**, 957 (2004).
27. J. W. B. Hershey, J. A. Leary, personal communication.
28. R. J. Jackson, *Eur. J. Biochem.* **200**, 285 (1991).
29. T. V. Pestova, V. G. Kolupaeva, *Genes Dev.* **16**, 2906 (2002).
30. S. Takyar, R. P. Hickerson, H. F. Noller, *Cell* **120**, 49 (2005).
31. B. T. Wimberly *et al.*, *Nature* **407**, 327 (2000).

32. We thank J. Frank and C. Spahn for making their maps available to us; H. Wang, A. Leschziner, P. Meurer-Grob, S. De Carlo, M. Peris, E. Galburt, S. Gradia, I. Macrae, W. Gilbert, K. Karbstein, R. Glaeser, J. Cate, and J. Hershey for advice and discussions; A. Avila-Sakar for EM support; and J. Fang for HeLa cytosol lysate. J.A.D. and E.N. are HHMI Investigators. B.S. is a Thai Scholar. The cryo-EM densities of eIF3 and eIF3-IRES (refined conformer-1) have been deposited to the Electron Microscopy Database (EMDB) with accession code EMD-1170 and EMD-1171, respectively.

Supporting Online Material

www.sciencemag.org/cgi/content/full/310/5753/1513/DC1
Materials and Methods
Figs. S1 to S6
Movie S1

17 August 2005; accepted 1 November 2005
10.1126/science.1118977